Analytical mean-field scaling theory of radio-frequency heating in a Paul trap

Y. S. Nam, E. B. Jones, and R. Blümel
Department of Physics, Wesleyan University, Middletown, Connecticut 06459-0155, USA

(Received 2 April 2014; revised manuscript received 28 May 2014; published 2 July 2014)

While the microscopic origins of radio-frequency (rf) heating of simultaneously stored, charged particles in a Paul trap are not yet understood in detail, a universal heating curve [J. D. Tarnas, Y. S. Nam, and R. Blümel, Phys. Rev. A **88**, 041401 (2013)] was recently discovered that collapses scaled rf heating data onto a single universal curve. Based on a simple analytical mean-field theory, we derive an analytical expression for the universal heating curve, which is in excellent agreement with numerical data. We find that for spherical clouds the universal curve depends only on a single scaling parameter, $\lambda = [q(N-1)]^{2/3}/T$, where N is the number of trapped particles, q is the Paul-trap control parameter, and T is the temperature.

DOI: 10.1103/PhysRevA.90.013402 PACS number(s): 37.10.Ty, 52.27.Jt

I. INTRODUCTION

Ever since the invention of the Paul trap in the 1950s [1], now used worldwide in scores of laboratories for applications ranging from ultrahigh accuracy atomic clocks [2] to quantum computers [3], experimentalists observed a curious phenomenon of ensembles of charged particles simultaneously stored in a Paul trap: radio-frequency (rf) heating [4–6]. Cooling in various forms, e.g., laser cooling [7] or buffer-gas cooling [8], has to be applied to counteract this heating phenomenon. While at this point in time we cannot yet predict rf heating rates as a function of particle number and trap parameters, we *are* able to offer an ordering principle, a universal curve [9], onto which scaled rf heating rates of stable, trapped particle clouds collapse. While in [9], based on extensive numerical simulation data, the heating curve was discovered phenomenologically, the purpose of this paper is to reveal the physical origin of the universal curve and derive analytically the scaling relationships that underlie the near-exact collapse of heating data onto the universal curve. Thus derivation and analytical investigation of this universal curve is the main objective of this paper.

Our paper is structured in the following way. In Sec. II, we summarize the most important Paul-trap equations and introduce the notation. In Sec. III, based on an analytical mean-field theory, we derive the general form of the universal heating curve. Further developing the general expression obtained in Sec. III, we derive, in Sec. IV, an explicit, analytical expression for the universal heating curve and compare it with numerical data. We find that the agreement is excellent. In Sec. V, we uncover an as yet hidden symmetry that explains why the universal curve is also universal in the Paul-trap q parameter. Thus we are able to show that for spherical clouds the universal curve depends only on a single scaling parameter, $\lambda = [q(N-1)]^{2/3}/T$, where N is the number of trapped particles, q is the Paul-trap control parameter, and T is the temperature of the cloud. This result is based on the mean-field theory developed in Sec. III, which rests on several assumptions and numerical observations, discussed and justified in detail in Sec. VI. In Sec. VII we summarize and conclude our paper.

II. PAUL-TRAP EQUATIONS

We start by briefly summarizing the most important Paul-trap equations [1,10,11], which also introduce and define the notation [9]. In dimensionless units, the coupled set of nonlinear Paul-trap equations is

$$\ddot{\vec{r}}_i + \gamma\dot{\vec{r}}_i + [a - 2q\,\sin(2t)]\begin{pmatrix} x_i \\ y_i \\ -2z_i \end{pmatrix} = \sum_{\substack{j=1\\ j\neq i}}^{N} \frac{\vec{r}_i - \vec{r}_j}{|\vec{r}_i - \vec{r}_j|^3}, \quad i = 1,\ldots,N, \tag{1}$$

where $\vec{r}_i = (x_i, y_i, z_i)$ is the position of the ith trapped particle, a and q are the dimensionless Paul-trap control parameters, and t is the dimensionless time. The set of equations (1) completely defines the damped dynamics of N particles in an ideal Paul trap and contains all the relevant physics of the heating problem. We also define the second moments s_x^2, s_y^2, and s_z^2, where s_x^2, e.g., is given by $s_x^2 = \sum_{i=1}^{N} x_i^2$, and analogously for the other two moments. In addition, we define $s^2 = s_x^2 + s_y^2 + s_z^2$. The total instantaneous energy of the set of particles described by (1) is

$$E(t) = E_{\text{kin}}(t) + E_{\text{trap}}(t) + E_{\text{Coul}}(t), \tag{2}$$

where

$$E_{\text{kin}}(t) = \frac{1}{2}\sum_{i=1}^{N} \dot{\vec{r}}_i^{\,2}, \tag{3}$$

$$E_{\text{trap}}(t) = \tfrac{1}{2}[a - 2q\,\sin(2t)]\left(s_x^2 + s_y^2 - 2s_z^2\right), \tag{4}$$

and

$$E_{\text{Coul}}(t) = \frac{1}{2}\sum_{\substack{i,j=1\\ i\neq j}}^{N} \frac{1}{|\vec{r}_i - \vec{r}_j|}. \tag{5}$$

Heating and cooling of the particles governed by (1) is best described by changes in the total energy $E(t)$ as a function of time t. Therefore, we compute $dE(t)/dt$ and write it in the form

$$\frac{dE(t)}{dt} = G(t) + S(t), \tag{6}$$

where

$$G(t) = -\gamma \sum_{i=1}^{N} \dot{\vec{r}}_i^{\,2} = -2\gamma E_{\rm kin}(t) \tag{7}$$

is the dissipative term, describing energy irretrievably lost from the system [since $E_{\rm kin}(t)$ is positive definite], and

$$S(t) = -2q\,\cos(2t)\big(s_x^2 + s_y^2 - 2s_z^2\big) \tag{8}$$

is the source of energy for the system. Since heating or cooling of the particles does not refer to the short-time fluctuations and oscillations of the energy on the scale of one trap cycle ($\Delta t = \pi$), but is a systematic, macroscopic effect that emerges when $E(t)$ is evaluated over many trap cycles, we introduce the cycle average $\bar{f}(t)$ of an arbitrary function $f(t)$ according to

$$\bar{f}(t) = \frac{1}{\pi}\int_t^{t+\pi} f(t')dt'. \tag{9}$$

In a situation where heating and cooling balance on average, i.e., a steady state is reached, it makes sense to define the long-time average of a dynamical function $f(t)$ as an average over many cycles according to

$$\bar{f} = \lim_{M\to\infty}\frac{1}{M\pi}\int_t^{t+M\pi} f(t')dt', \tag{10}$$

where, in steady state, the zero of time t is arbitrary. In steady state, there is no net long-time gain or loss of system energy. Therefore, we have

$$\overline{\frac{dE}{dt}} = \bar{G} + \bar{S} = 0, \tag{11}$$

from which it follows immediately that the average heating power $\bar{S}$ may be expressed with the help of the cooling power $\bar{G}$ via

$$\bar{S} = -\bar{G} = 2\gamma \bar{E}_{\rm kin}. \tag{12}$$

A consequence of (12) is that, given γ, it allows us to compute the heating power $\bar{S}$ as soon as we have an expression for $\bar{E}_{\rm kin}$. We derive it in pseudopotential approximation [1,4,12]. The advantage of the pseudopotential approximation is that it allows access to average properties of the particle dynamics, approximately keeping track of the time dependence of the particles' motion during a trap cycle. Splitting the trajectory of particle number i into its macromotion part $\vec{R}_i = (X_i,Y_i,Z_i)$ and its micromotion part $\vec{\chi}_i$ [12], we may integrate analytically over the micromotion part of the trajectories when computing cycle averages and arrive at an expression for $\bar{E}_{\rm kin}$ that contains only the macromotion parts of the particle trajectories. We obtain [9]

$$\bar{E}_{\rm kin} = \frac{1}{2}\sum_{i=1}^{N}\Bigg[\left(1+\frac{q^2}{8}\right)\big(\overline{\dot{X}_i^2} + \overline{\dot{Y}_i^2}\big) + \left(1+\frac{q^2}{2}\right)\overline{\dot{Z}_i^2} + \frac{q^2}{2}\big(\overline{X_i^2} + \overline{Y_i^2}\big) + 2q^2\overline{Z_i^2}\Bigg], \tag{13}$$

where the overlines indicate long-time averages according to (10), and the terms proportional to q^2 are due to the micromotion, thus taking the micromotion into account. Assuming ergodicity, we may replace the time averages by ensemble averages and obtain

$$\bar{E}_{\rm kin} = \frac{1}{2}\sum_{i=1}^{N}\Bigg[\left(1+\frac{q^2}{8}\right)\big(\langle\dot{X}_i^2\rangle + \langle\dot{Y}_i^2\rangle\big) + \left(1+\frac{q^2}{2}\right)\langle\dot{Z}_i^2\rangle + \frac{q^2}{2}\big(\langle X_i^2\rangle + \langle Y_i^2\rangle\big) + 2q^2\langle Z_i^2\rangle\Bigg], \tag{14}$$

where ensemble averages are denoted by the angular brackets $\langle\cdots\rangle$. Given the chaotic nature of the dynamics of a trapped Coulomb gas [10,11], replacing time averages with ensemble averages is expected to be an excellent approximation.

III. MEAN-FIELD THEORY

In order to evaluate the ensemble averages in (14), we need the distribution function $f(\vec{V}_1,\ldots,\vec{V}_N;\vec{R}_1,\ldots,\vec{R}_N)$, where $\vec{V}_i$ is the macromotion velocity of particle number i, i.e.,

$$\vec{V}_i = \dot{\vec{R}}_i. \tag{15}$$

Since positions and velocities are not coupled in the N-particle Hamiltonian of the trap, the distribution function separates into a velocity-dependent part and a space-dependent part according to

$$f(\vec{V}_1,\ldots,\vec{V}_N;\vec{R}_1,\ldots,\vec{R}_N) = f_V(\vec{V}_1,\ldots,\vec{V}_N)\,f_R(\vec{R}_1,\ldots,\vec{R}_N), \tag{16}$$

where

$$f_V(\vec{V}_1,\ldots,\vec{V}_N) = (2\pi T)^{-3N/2}\exp\left(-\frac{1}{2T}\sum_{i=1}^{N}\vec{V}_i^2\right). \tag{17}$$

In (17) we introduced the temperature T of the trapped particle clouds. This may look like a dangerous proposition given that the dynamics (1) of the trapped particles are explicitly time dependent. Indeed, the temperature of the cloud changes during a trap cycle and may even be different in the radial and the z directions. However, the concept of temperature is well defined if it refers to the temperature of the macromotion [13] and care is taken to evaluate T always at the same phase during a trap cycle, i.e., T has to be evaluated stroboscopically. Moreover, focusing, for now, on the case of spherical clouds eliminates the problem of different temperatures in different directions and a single temperature T, as used in (17), is well defined.

The pseudo-oscillator energy of the macromotion is

$$V_{\rm osc}(\vec{R}_1,\ldots,\vec{R}_N) = \frac{1}{2}\sum_{i=1}^{N}\big(\omega_x^2X_i^2 + \omega_y^2Y_i^2 + \omega_z^2Z_i^2\big), \tag{18}$$

where [11]

$$\omega_x^2 = \omega_y^2 \approx a + q^2/2, \quad \omega_z^2 \approx 2(q^2 - a). \tag{19}$$

The Coulomb energy of the macromotion is

$$V_{\rm Coul}(\vec{R}_1,\ldots,\vec{R}_N) = \sum_{\substack{i,j=1\\ j>i}}^{N}\frac{1}{|\vec{R}_i - \vec{R}_j|}, \tag{20}$$

and the distribution function of the macromotion positions is

$$f_R(\vec{R}_1,\ldots,\vec{R}_N) = \mathcal{N}_R \exp\left\{-\frac{1}{T}[V_{\rm osc}(\vec{R}_1,\ldots,\vec{R}_N)+V_{\rm Coul}(\vec{R}_1,\ldots,\vec{R}_N)]\right\}, \tag{21}$$

where

$$\mathcal{N}_R = \left[\int \exp\left\{-\frac{1}{T}[V_{\rm osc}(\vec{R}_1,\ldots,\vec{R}_N) + V_{\rm Coul}(\vec{R}_1,\ldots,\vec{R}_N)]\right\}d^{3N}\vec{R}\right]^{-1}. \tag{22}$$

Instead of including all particle-particle correlations in our analytical analysis, we imagine that we focus on a single trapped particle at position $\vec{R}$ with velocity $\vec{V}=\dot{\vec{R}}$, moving in the mean field set up by the other $N-1$ particles. This defines a mean-field picture in which all correlations are neglected and all particles are described by the same single-particle distribution function

$$f(\vec{V},\vec{R}) = \beta(\vec{V})\rho(\vec{R}), \tag{23}$$

where $\beta(\vec{V})$ describes the probability distribution of velocity and $\rho(\vec{R})$ is the space-distribution function of any one of the particles in the cloud. The velocity distribution function is the single-particle version of (17), i.e.,

$$\beta(\vec{V}) = \frac{1}{(2\pi T)^{3/2}}\exp\left(-\frac{1}{2T}\vec{V}^2\right) = \beta_x(V_x)\beta_y(V_y)\beta_z(V_z), \tag{24}$$

where

$$\beta_l(V_l) = \frac{1}{(2\pi T)^{1/2}}\exp\left(-\frac{1}{2T}V_l^2\right), \tag{25}$$

and $l=x$, y, or z. The single-particle space-distribution function is

$$\rho(\vec{R}) = \mathcal{N}\exp\left\{-\frac{1}{T}[V_{\rm osc}(\vec{R})+V_{\rm Coul}(\vec{R})]\right\}, \tag{26}$$

where

$$\mathcal{N} = \left[\int \exp\left\{-\frac{1}{T}[V_{\rm osc}(\vec{R})+V_{\rm Coul}(\vec{R})]\right\}d^3\vec{R}\right]^{-1} \tag{27}$$

is the normalization factor,

$$V_{\rm osc}(\vec{R}) = \frac{1}{2}\left(\omega_x^2X^2+\omega_y^2Y^2+\omega_z^2Z^2\right), \tag{28}$$

and

$$V_{\rm Coul}(\vec{R}) = (N-1)\int\frac{\rho(\vec{R}')d^3\vec{R}'}{|\vec{R}-\vec{R}'|}. \tag{29}$$

Using (29) in (26), we obtain an integral equation for ρ according to

$$\rho(\vec{R}) = \mathcal{N}[\rho]\exp\left\{-\frac{1}{T}\left[V_{\rm osc}(\vec{R})+(N-1)\int\frac{\rho(\vec{R}')d^3\vec{R}'}{|\vec{R}-\vec{R}'|}\right]\right\}, \tag{30}$$

where the notation $\mathcal{N}[\rho]$ indicates that the normalization constant (27) via (29) is a functional of ρ. We now notice that $V_{\rm osc}$ and $V_{\rm Coul}$ are homogeneous functions [12] of degrees 2 and -1, respectively. Therefore, scaling $\vec{R}$ according to

$$\vec{R} = (N-1)^{1/3}\vec{u}, \tag{31}$$

together with $\rho(\vec{R})d^3\vec{R} = \rho(\vec{u})d^3\vec{u}$, allows us to write (30) in the form

$$\rho(\vec{u}) = \hat{\mathcal{N}}[\rho(\vec{u})]\exp\left\{-\frac{(N-1)^{2/3}}{T}\left[V_{\rm osc}(\vec{u}) + \int\frac{\rho(\vec{u}')d^3\vec{u}'}{|\vec{u}-\vec{u}'|}\right]\right\}, \tag{32}$$

where

$$\hat{\mathcal{N}}[\rho] = \left[\int\exp\left\{-\frac{(N-1)^{2/3}}{T}\left[V_{\rm osc}(\vec{u}) + \int\frac{\rho(\vec{u}')d^3\vec{u}'}{|\vec{u}-\vec{u}'|}\right]\right\}d^3\vec{u}\right]^{-1} \tag{33}$$

is the new normalization constant. Equations (32) and (33) show clearly that $\rho(\vec{u})$ is not a function of N and T separately, but depends only on the ratio

$$\kappa = \frac{(N-1)^{2/3}}{T}. \tag{34}$$

Therefore, we may write

$$\rho(\vec{u}) = \rho(\vec{u};a,q;\kappa). \tag{35}$$

In [9] we defined the scaled heating rate

$$h = \frac{\bar{E}_{\rm kin}}{\bar{E}_{\rm kin}^{\rm nig}}, \tag{36}$$

where

$$\bar{E}_{\rm kin}^{\rm nig} = \frac{N}{2}\left\{\left[\left(1+\frac{q^2}{8}\right)\omega_x^2+\frac{q^2}{2}\right]\langle X^2\rangle + \left[\left(1+\frac{q^2}{8}\right)\omega_y^2+\frac{q^2}{2}\right]\langle Y^2\rangle + \left[\left(1+\frac{q^2}{2}\right)\omega_z^2+2q^2\right]\langle Z^2\rangle\right\} \tag{37}$$

is the cycle-averaged kinetic energy of the trapped particles with the Coulomb interaction switched off (noninteracting gas). We showed that for fixed a and q a universal curve results, independent of N and T, when h is plotted against

$$\sigma = \hat{s}/s_c. \tag{38}$$

Here,

$$\hat{s} = \sqrt{\langle s^2\rangle} = \left\{\sum_{i=1}^{N}\left[\langle X_i^2\rangle + \langle Y_i^2\rangle + \langle Z_i^2\rangle\right]\right\}^{1/2}, \tag{39}$$

if $\hat{s}$ is evaluated at the end of each trap cycle, and s_c is the root-mean-square size of the crystal. Assuming spherical symmetry and a homogeneous charge distribution, we evaluate s_c in pseudo-oscillator approximation, where the confining field is a harmonic oscillator with oscillator frequencies $\omega_x=\omega_y=\omega_z=\omega$, where, according to (19), $\omega\approx q$. In this case, the charge density ρ_c of the crystal is a constant for $0 \leqslant R \leqslant R_c$ and 0 for $R > R_c$, where R_c is the radius of the crystal. To determine R_c, we need to equate the mechanical restoring force $F = \omega^2 R$ of the oscillator with the Coulomb force, E, at $R = R_c$. From $\vec{\nabla} \cdot \vec{E} = 4\pi\rho_c$ we obtain

$$\rho_c = \frac{3q^2}{4\pi}, \tag{40}$$

and from $N = 4\pi\rho_c R_c^3/3$ we obtain

$$R_c = (N/q^2)^{1/3}. \tag{41}$$

This is all we need to compute

$$s_c = \left\{4\pi\rho_c \int_0^{R_c} r^4\, dr\right\}^{1/2} = \left(\frac{3}{5q^{4/3}}\right)^{1/2} N^{5/6}. \tag{42}$$

On the basis of (35) it is now straightforward to provide a theoretical underpinning for what in [9] was a purely heuristic procedure. Defining

$$\vec{M}^{(\nu)} = \frac{1}{N}\sum_{i=1}^{N}\left(X_i^\nu Y_i^\nu Z_i^\nu\right) = (\langle X^\nu\rangle\langle Y^\nu\rangle\langle Z^\nu\rangle) \tag{43}$$

as the νth moments of the macromotion coordinates and

$$\vec{\mu}^{(\nu)} = \int \left(u_x^\nu u_y^\nu u_z^\nu\right) \rho(\vec{u};a,q;\kappa) d^3\vec{u} \tag{44}$$

as the νth moments of the scaled density $\rho(\vec{u};a,q;\kappa)$, we obtain with (31)

$$\vec{M}^{(2)} = (N-1)^{2/3}\, \vec{\mu}^{(2)}(a,q;\kappa). \tag{45}$$

With (43), (44), and (45), we may express $\hat{s}$ in (39) in the form

$$\begin{aligned}\hat{s} &= \left\{N\left[M_x^{(2)} + M_y^{(2)} + M_z^{(2)}\right]\right\}^{1/2}\\ &= [N(N-1)^{2/3}]^{1/2}\left[\mu_x^{(2)} + \mu_y^{(2)} + \mu_z^{(2)}\right]^{1/2},\end{aligned} \tag{46}$$

which, for large N, where $(N-1)/N \approx 1$, may also be written as

$$\hat{s} = N^{5/6}\left[\mu_x^{(2)} + \mu_y^{(2)} + \mu_z^{(2)}\right]^{1/2}. \tag{47}$$

We now see that, when computing σ defined in (38) as the ratio of $\hat{s}$ defined in (47) and s_c defined in (42), the factor $N^{5/6}$ cancels, and since the moments μ in (47) are functions of a, q, and κ only, we obtain the result that

$$\sigma = \sigma(a,q;\kappa) \tag{48}$$

is a function of a, q, and κ only, and is not dependent on N and T separately. We also note that

$$\frac{1}{T}\vec{M}^{(2)} = \kappa\vec{\mu}^{(2)}(a,q;\kappa) \tag{49}$$

is a function of a, q, and κ only. Assuming the same temperature in all three directions, we have

$$\langle \dot{X}^2\rangle = \langle \dot{Y}^2\rangle = \langle \dot{Z}^2\rangle = T. \tag{50}$$

With this information in hand, we define and compute

$$\begin{aligned}\epsilon(a,q;\kappa) &= \frac{1}{NT}\bar{E}_{\text{kin}}\\ &= \frac{1}{2}\left[3 + \frac{3}{4}q^2 + \frac{\kappa q^2}{2}\left(\mu_x^{(2)} + \mu_y^{(2)}\right) + 2\kappa q^2\mu_z^{(2)}\right]\end{aligned} \tag{51}$$

and

$$\begin{aligned}\epsilon_0(a,q;\kappa) = \frac{1}{NT}\bar{E}_{\text{kin}}^{\text{nig}} = \frac{\kappa}{2}\Bigg\{&\left[\left(1+\frac{q^2}{8}\right)\omega_x^2 + \frac{q^2}{2}\right]\mu_x^{(2)}\\ &+\left[\left(1+\frac{q^2}{8}\right)\omega_y^2 + \frac{q^2}{2}\right]\mu_y^{(2)}\\ &+\left[\left(1+\frac{q^2}{2}\right)\omega_z^2 + 2q^2\right]\mu_z^{(2)}\Bigg\}.\end{aligned} \tag{52}$$

Therefore, we have

$$h(a,q;\kappa) = \frac{\epsilon(a,q;\kappa)}{\epsilon_0(a,q;\kappa)}, \tag{53}$$

i.e., $h(a,q;\kappa)$ is a function of a, q, and κ only. Thus, for fixed a and q, as observed numerically in [9], a one-parameter manifold, i.e., the universal curve [9], results when h is plotted against σ.

IV. HEATING CURVE: EXPLICIT ANALYTICAL FORM AND COMPARISON WITH NUMERICAL DATA

At this point, because of κ scaling, we explained why the heuristic scaling procedure outlined in [9] "works," i.e., why, for fixed a,q, the heating data of trapped, charged particle clouds all collapse onto one single, universal curve. What is missing is an explicit, analytical formula of the universal heating curve to be compared with the numerical heating data. Moreover, the numerical results in [9] indicate that the heating curves for different q may also collapse onto each other. To find the analytical form of the heating curve and to check whether there is yet another scaling hidden in the particle dynamics that may account for the observed near degeneracy of heating curves for different q, we have to solve (32) analytically. To accomplish this, we restrict ourselves to the spherically symmetric case $\omega_x = \omega_y = \omega_z$, which, according to (19), occurs for $a \approx q^2/2$. In this case we have

$$\omega_x = \omega_y = \omega_z = q \tag{54}$$

and

$$\rho(u) = \hat{N}\, \exp\left[-\kappa\left(\frac{1}{2}q^2u^2 + \int \frac{\rho(u')d^3\vec{u}'}{|\vec{u}-\vec{u}'|}\right)\right]. \tag{55}$$

The integral term in (55) may be reduced to an expression containing only one-dimensional integrals according to

$$\int \frac{\rho(u')d^3\vec{u}'}{|\vec{u}-\vec{u}'|} = 4\pi\left[\frac{1}{u}\int_0^u (u')^2\rho(u')du' + \int_u^\infty u'\rho(u')du'\right]. \tag{56}$$

Even with the simplification of spherical symmetry, Eq. (32) is still a nonlinear integral equation. Therefore, we look for an approximate solution of (32) in the form of a Gaussian,

$$\rho(\vec{u}) = \tilde{\mathcal{N}} \exp(-\alpha u^2), \tag{57}$$

where the normalization constant $\tilde{\mathcal{N}}$ is given by

$$\tilde{\mathcal{N}} = (\alpha/\pi)^{3/2}, \tag{58}$$

and $\alpha > 0$ has to be determined such that (57) is an approximate solution of (32). The form (57) of ρ now allows us to compute the integrals in (56) explicitly. Up to second order in u we obtain

$$\int \frac{\rho(u')d^3\vec{u}'}{|\vec{u}-\vec{u}'|} = 4\pi\tilde{\mathcal{N}}\left[\left(\frac{1}{2\alpha}\right) - \frac{1}{6}u^2\right]. \tag{59}$$

Therefore, up to second order in u, the integral equation (32) now reads

$$\begin{aligned}&\tilde{\mathcal{N}} \exp(-\alpha u^2)\\ &\quad = \hat{\mathcal{N}} \exp\left\{-\kappa\left[\frac{1}{2}q^2u^2 + \frac{2\pi}{\alpha}\tilde{\mathcal{N}} - \frac{2\pi}{3}\tilde{\mathcal{N}}u^2\right]\right\}.\end{aligned} \tag{60}$$

The exponents and normalization factors are consistent if

$$\alpha = \frac{1}{2}\kappa q^2 - \left(\frac{2\kappa}{3\sqrt{\pi}}\right)\alpha^{3/2} \tag{61}$$

and

$$\hat{\mathcal{N}} = \tilde{\mathcal{N}} \exp\left[\left(\frac{2\pi}{\alpha}\right)\kappa\tilde{\mathcal{N}}\right]. \tag{62}$$

Moving the constant term in (61) to the left-hand side and squaring transforms (61) into a cubic equation whose solutions may be stated analytically [14]. However, it is more instructive to investigate the solutions of (61) for fixed N in the limits of low and high temperatures. For $T \to \infty$, we have $\kappa \to 0$ and $\alpha \to 0$. Therefore, in this case, we may neglect the term proportional to $\alpha^{3/2}$ in (61) and obtain

$$\alpha = \tfrac{1}{2}\kappa q^2 \quad \text{for } \kappa \to 0. \tag{63}$$

For $T \to 0$, we have $\kappa \to \infty$. In this case we may neglect the left-hand side of (61) with respect to the right-hand side and obtain

$$\alpha = \left(\frac{3q^2\sqrt{\pi}}{4}\right)^{2/3} \quad \text{for } \kappa \to \infty. \tag{64}$$

This is an interesting, but expected, result. In the limit of $T \to 0$, for fixed N, the cloud of trapped particles will transition into the crystal state [10,11], which, due to the Coulomb repulsion, has a finite extent. This is reflected in the fact that, according to (64), α is a constant in this limit.

Once α is computed, either approximately according to (63) or (64), or exactly by solving the associated cubic equation [14], the normalization constants $\tilde{\mathcal{N}}$ and $\hat{\mathcal{N}}$ are also known and $\rho(u,\kappa)$ is completely determined.

We now return to the computation of h. In the spherical case we have

$$\mu_x^{(2)} = \mu_y^{(2)} = \mu_z^{(2)} = \frac{1}{2\alpha}. \tag{65}$$

Using this together with (54) in (53), we obtain

$$h(q;\kappa) = \frac{2\alpha(q;\kappa)\left(1+\frac{q^2}{4}\right) + \kappa q^2}{2\kappa q^2\left(1+\frac{q^2}{8}\right)}. \tag{66}$$

According to construction, and for fixed N, we expect that $h \to 1$ for $T \to \infty$. This is indeed the case. Using (63), applicable in the case $T \to \infty$, we obtain $h = 1$. In [9] we showed that $h \approx 1/2$ in the crystal state where $T = 0$ and $\kappa \to \infty$. Since, according to (64), α is a constant in this case, we obtain $h = 1/[2(1+q^2/8)] \approx 1/2$ in this limit. Thus our analytical result (66) reproduces both limits of the universal curve.

In order to compare our analytical universal curve with the numerical data of [9], we need an analytical expression for $\sigma(q;\kappa)$. In [9] we normalized the size of the particle cloud to the size of the crystal. In our analytical model the consistent, analogous procedure is to normalize the size of the particle cloud at finite T to the size of the cloud at $T = 0$. Since

$$\begin{aligned}\langle s^2\rangle &= N\langle X^2+Y^2+Z^2\rangle = N(N-1)^{2/3}\langle u^2\rangle\\ &= \left(\frac{3}{2\alpha}\right)N(N-1)^{2/3},\end{aligned} \tag{67}$$

we have

$$\sigma = \sqrt{\frac{\alpha(q;\kappa=\infty)}{\alpha(q;\kappa)}}, \tag{68}$$

where $\alpha(q;\kappa=\infty)$ is stated in (64).

We are now ready to plot the universal curve and compare with the numerical data. The result is shown in Fig. 1. The smooth line is the universal heating curve (66); the data points are the scaled heating rates imported from Fig. 3 of [9]. We see that, especially for small σ, i.e., in the low-temperature regime, the agreement of the analytical prediction with the numerical simulation data is near perfect. Deviations occur only for large σ, i.e., in the high-temperature regime. This observation, in fact, is odd, since the agreement is expected to be better in the more "trivial" high-temperature regime where the interacting Coulomb gas is expected to become a noninteracting gas of isolated particles, perfectly described

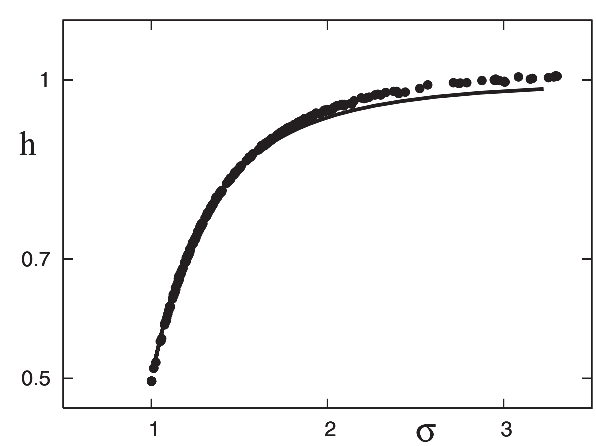

FIG. 1. Scaled heating rate h versus scaled cloud size σ. Solid line: analytical scaled heating rate (66) versus analytical cloud size (68). Plot symbols: numerical data for scaled heating rates obtained by simulating the dynamics of $N = 50,100,200,500$ particles simultaneously stored in an ideal Paul trap with $q = 0.2$ and $a = q^2/2$ (data transferred from Fig. 3 of [9]). The analytical curve is in excellent agreement with the numerical data.

by $\bar{E}_{\text{kin}}^{\text{nig}}$ [see (37)]. Since h is normalized to $\bar{E}_{\text{kin}}^{\text{nig}}$, we expect perfect agreement. As already mentioned in [9], the deviation may have two reasons: (a) our use of the approximate pseudo-oscillator frequencies (19) and (b) that for $a = q^2/2$ the particle cloud, because of higher-order corrections, is not perfectly spherical. In fact, for $q = 0.2$, $a = q^2/2$, the values of a and q used in [9], the exact pseudo-oscillator frequencies are $\omega_x = \omega_y = 0.202$ and $\omega_z = 0.205$. This shows that (i) the particle cloud is not perfectly spherical and (ii) the deviation of the exact pseudo-oscillator frequencies from their lowest-order approximations (19) is of the order of a few percent. Since the deviation of the analytical universal curve from the trend of the numerical data in Fig. 1 is also only of the order of 4%, this may well contribute to the discrepancy. Preferring simplicity over exactness, we used the approximate ω values to obtain the simple, straightforward analytical form for h in (66).

V. UNCOVERING A HIDDEN, ADDITIONAL SCALING

In [9] we found that the heating data for $q = 0.3$ almost collapse onto the heating curve for $q = 0.2$, indicating that an additional, unexpected scaling might exist. This is indeed the case. Let us introduce the scaling $\alpha = q^{4/3}w$, which turns (61) into

$$w = \frac{1}{2}\kappa q^{2/3} - \left(\frac{2\kappa}{3\sqrt{\pi}}\right)q^{2/3}w^{3/2}. \tag{69}$$

Defining

$$\lambda = \kappa q^{2/3} = \frac{(N-1)^{2/3}}{T}q^{2/3}, \tag{70}$$

we have

$$w = \frac{1}{2}\lambda - \left(\frac{2\lambda}{3\sqrt{\pi}}\right)w^{3/2}. \tag{71}$$

Unlike (61), which depends on q and κ separately, Eq. (71) depends only on the single scaling parameter λ. Thus we may write the solution of (71) in the form $w(\lambda)$.

Returning now to the evaluation of σ in (68), we find

$$\sigma(\lambda) = \left(\frac{3q^2\sqrt{\pi}}{4}\right)^{1/3} \Big/ [\alpha(q;\kappa)]^{1/2} = \left(\frac{3\sqrt{\pi}}{4}\right)^{1/3} \Big/ w(\lambda)^{1/2}, \tag{72}$$

which scales in the single parameter λ. Similarly, expressing h in (66) in terms of $w(\lambda)$, we find

$$h(q;\lambda) = \frac{2q^{4/3}w(\lambda)(1+q^2/4)+\kappa q^2}{2\kappa q^2(1+q^2/8)} = \frac{2w(\lambda)(1+q^2/4)+\lambda}{2\lambda(1+q^2/8)}. \tag{73}$$

For small q, we may neglect the terms quadratic in q in (73). In this case, just like σ in (72), h depends on the single scaling parameter λ only. In fact, for $q \leqslant 0.4$, the analytical curves $h(q;\lambda)$ collapse approximately onto one single curve and cannot be distinguished as separate curves on the scale of Fig. 1. Thus we explained the near degeneracy of heating curves for different q values found in [9] as due to the fact that both h and σ scale significantly only in the single parameter λ. Thus we showed that the heating data of spherical clouds confined in a spherical trap all collapse onto a single, universal heating curve.

VI. DISCUSSION

In order to predict absolute heating rates of charged-particle clouds in a Paul trap, our ultimate goal is to evaluate $S(t)$, the source term defined in (8), directly as a function of trap parameters. This, however, is extremely difficult and depends on both microscopic and macroscopic details of the trapped particles' dynamics. Concerning the global characteristics of the dynamics, we found that it makes a substantial difference whether the particle dynamics are integrable or not. For instance, as reported in [9], replacing the two-body Coulomb interaction in (1) with an integrable, harmonic two-body force results in particle clouds that do not heat. This shows that the global properties of the dynamics are an essential ingredient for understanding rf heating. However, it has also been suggested in the literature that close particle-particle collisions are a source of rf heating [15–17]. This is corroborated by our numerical simulations with two-body Coulomb interactions, which show that large, sudden changes in $E(t)$ are always accompanied by close particle-particle collisions. However, in view of our experience with integrable two-body interactions, it is clear that close collisions are only a necessary condition for rf heating to occur, since close collisions certainly do occur in the case of the nonheating, harmonic two-body force, which does *not* exhibit rf heating [9]. Therefore, we are led to the conclusion that both close collisions and nonintegrable dynamics are necessary ingredients for understanding the rf heating phenomenon. Since both nonintegrability and nonlinear collisions are difficult to deal with analytically, this explains why it is so difficult to evaluate $S(t)$, and, by extension, $\bar{S}$. Applied to the present case, for example, neglecting collisions, but taking the micromotion into account, it is straightforward to show that $\bar{S} = 0$, a useless result that does not explain the rf heating phenomenon, but *does* point to the importance of two-body collisions as a necessary ingredient for the explanation of rf heating.

Side-stepping direct evaluation of $S(t)$, we took a different route, evaluating instead the dissipative term $G(t)$, which, according to (7) is simply connected with $E_{\text{kin}}(t)$ and is much more readily accessible. The price to pay is that $S(t)$ and $G(t)$ are directly connected only in steady state, i.e., when a balance exists between rf heating and dissipative cooling. Nevertheless, this allows us to determine the universal scaling behavior of trapped particle clouds in the form of a universal curve that all future rf heating theories have to satisfy and may be used to constrain these theories.

An important condition for our method to work is the existence of a steady-state solution of (1). In order to prove the existence of a steady state in the kinetic energy $E_{\text{kin}}(t)$, we show, in Fig. 2, $E_{\text{kin}}(n\pi)$ as a function of trap cycle number n for the case $N = 20$, $a = 0.02$, $q = 0.2$, and $\gamma = 4 \times 10^{-4}$. Figure 2 shows that after an initial transient, lasting for about 3000 trap cycles (due to choosing a random initial condition for this cloud at $t = 0$), $E_{\text{kin}}(n\pi)$ settles down into a steady state, fluctuating around its long-time average $\bar{E}$. We checked

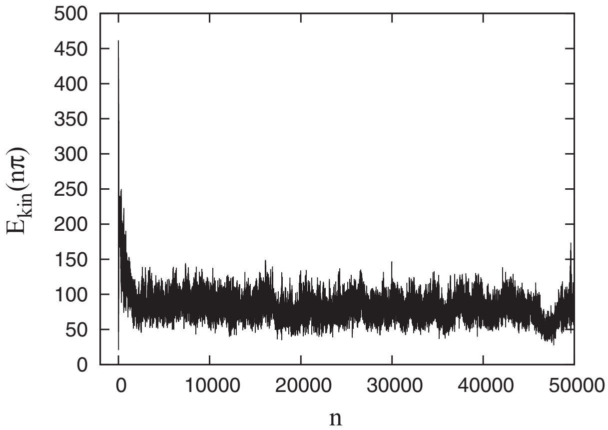

FIG. 2. Stoboscopic kinetic energy $E_{\mathrm{kin}}(n\pi)$ of a 20-particle cloud as a function of cycle number n. After an initial transient, lasting for about 3000 cycles, $E_{\mathrm{kin}}(n\pi)$ settles down to a steady state, exhibiting fluctuations around a constant value $\bar{E}_{\mathrm{kin}}$.

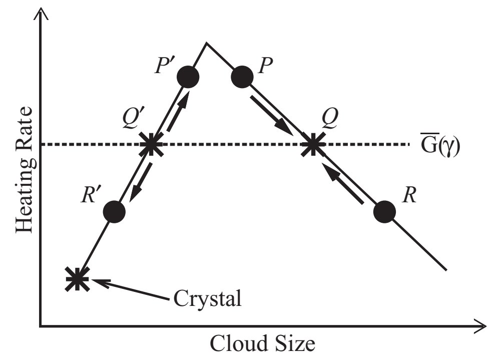

FIG. 3. Schematic diagram of rf heating rate vs cloud size (rate function) in the presence of cooling power $\bar{G}(\gamma)$. The rate function has the shape of a tent consisting of two wings with decreasing rf heating power as a function of increasing (right wing) cloud size or decreasing (left wing) cloud size. Starting a cloud in states corresponding to points P or R on the right wing of the rate function, the corresponding clouds move toward Q. Starting a cloud in a state corresponding to point R', cooling wins over rf heating and the cloud quickly crystallizes. Starting a cloud in point P', rf heating wins over cooling, the cloud "goes over the top" of the rate function, and settles in the vicinity of Q. Thus Q is a stable stationary point, while Q' is unstable. The diagram also shows that a runaway event in which the cloud expands due to uncontrollable heating is impossible for any γ, since the cloud *always* ends up in one of the two possible, stable, stationary states, either in Q or as a crystal.

explicitly, by continuing to run this simulation for 10^5 cycles (not shown in Fig. 2), that (a) the upward spike at $n \approx 50\,000$ is only a local fluctuation and (b) the stationary pattern exhibited in Fig. 2 continues as shown in Fig. 2 without indication of any runaway heating, strongly suggesting that for $n \gtrsim 3000$, rf heating and cooling are always balanced on average. While Fig. 2 shows an isolated example of the existence of a steady state for a single N,a,q,γ combination, of the literally thousands of N,a,q,γ combinations for which we performed numerical heating simulations, spherical or not, we never found a single example that would have shown runaway heating.

At first glance, the eventual balance of heating and cooling, i.e., the existence of stationary states for *any* damping parameter $\gamma > 0$, may seem surprising. However, given the fact that numerical evidence firmly establishes that the rf heating rate of trapped particle clouds decreases with cloud size (see, e.g., [10]), this phenomenon is no longer surprising. Figure 3, a schematic sketch for the purpose of increasing clarity, illustrates the connection between rf heating rate and cloud size, in the following referred to as the rate function. We see that the overall shape of the rate function, qualitatively, has the form of a tent. There exists a cloud size that produces a maximal heating rate (tip of the tent), and the heating rate decreases to both sides of the tip. Let us first focus on large clouds (right wing of the rate function). Let us also assume that cooling is switched on with a damping constant γ that results in the cooling power $\bar{G}(\gamma)$, indicated by the dashed line in Fig. 3. If in this situation, we start with a cloud whose size corresponds to point R on the rate function, the rf heating power produced by the cloud is insufficient to counteract the cooling power $\bar{G}$. Consequently, kinetic energy is drained from the cloud, and its size shrinks. Indicated by the arrow in Fig. 3, the cloud will move from point R toward point Q. Conversely, if we start with a smaller cloud, corresponding to point P, the rf heating power of the cloud will exceed the cooling power $\bar{G}$. As a consequence, the kinetic energy of the cloud will increase, the cloud will expand, and, as indicated by the arrow in Fig. 3, will move toward point Q. Thus clouds larger than those corresponding to point Q will cool, shrink, and move toward Q, and clouds smaller than those corresponding to point Q will heat, expand, and also move toward Q. Thus, for given damping constant γ, point Q is a *stable* stationary point. It is apparent that no matter how small γ, a stable stationary point always exists on the right wing of the rate function.

A technical point is in order here. We did not extend the plot of the rate function toward very large cloud sizes, since, at this point in time, we do not know whether the rate function actually intersects the cloud-size axis, or approaches it asymptotically. Clearing up this question is computationally expensive, since the smaller the damping constant γ, the longer the simulations have to run in order to establish the stationary point Q. Luckily, for the statement that Q exists on the right wing of the rate function, independent of the size of γ (as long as γ is small enough so that $\bar{G}$ is below the tip of the rate function), it does not matter whether the rate function intersects the cloud-size axis, or whether it only approaches it asymptotically. Based on this discussion, and, in particular, based on the decreasing nature of the rate function for large cloud sizes (see Fig. 3), a runaway event, in which from some time t^* on the rf heating power beats the cooling power (on average) for all times $t > t^*$, leading to an ever-expanding cloud, is strictly impossible.

Let us now discuss what happens if we start the cloud in point R' on the left wing of the rate function. In this case the rf heating power of the cloud is smaller than the cooling power. Therefore, the cloud will lose kinetic energy, and become even smaller. In fact, indicated by the arrow in Fig. 3, the cloud will move away from point Q' and rapidly collapse into the crystal state. Conversely, a cloud started in point P' has more rf heating power than can be counteracted by the cooling power $\bar{G}$. Thus, as indicated by the arrow in Fig. 3, the cloud will move away from Q', reach the top of the rate function, and keep expanding, but with *decreasing* rf heating power, until it reaches the stationary point Q. From thereon, it will fluctuate around Q, just like a cloud that was started on the right wing of the rate function. Therefore, clouds started on the left wing of the rate function have two possibilities: either they collapse into the crystalline state (a stationary point), or they go "over the top" and end up at the stationary point Q. In any case, no matter where we start the cloud, on the left wing or on the right wing, the cloud will always end up in a stationary state and *not* exhibit a runaway heating event. This is important for our analysis, because our theory depends crucially on the existence of the stable, stationary point Q. We remark that Q' corresponds to an unstable state, since the slightest perturbation, either up or down on the rate function, sends the cloud either to Q or into the crystalline state.

In many places in this paper we make extensive use of the pseudopotential approximation [1,4,12] and the question is whether its use is justified in the present context. The essential feature of the pseudopotential method is to decompose the trajectory $x_i(t)$ of particle number i in the trap into a slow, guiding-center motion $\vec{R}_i(t)$ and a fast oscillatory motion $\vec{\chi}_i(t)$ according to

$$\vec{x}_i(t) = \vec{R}_i(t) + \vec{\chi}_i(t), \tag{74}$$

where

$$\vec{R}_i(t) = \begin{pmatrix} X_i(t) \\ Y_i(t) \\ Z_i(t) \end{pmatrix}, \tag{75}$$

as introduced in Sec. II, and

$$\vec{\chi}_i(t) = \begin{pmatrix} \xi_i(t) \\ \eta_i(t) \\ \zeta_i(t) \end{pmatrix}. \tag{76}$$

As discussed in Sec. II, the motion described by $\vec{R}(t)$ is referred to as the *macromotion* and the motion described by $\vec{\chi}(t)$ is referred to as the *micromotion*. The two names are chosen, since, in general, the macromotion describes the large-amplitude excursions of a trapped particle, while the micromotion describes the small-amplitude, high-frequency oscillations of a trapped particle around the macromotion. Thus the basis of (74) is a time-scale analysis, which allows an approximate solution of (1) of the form (74), where $\vec{R}_i(t)$ satisfies the coupled set of equations [12]

$$\ddot{\vec{R}}_i + \gamma\dot{\vec{R}}_i + \begin{pmatrix} \omega_x^2 X_i \\ \omega_y^2 Y_i \\ \omega_z^2 Z_i \end{pmatrix} = \sum_{\substack{j=1 \\ j\neq i}}^{N} \frac{\vec{R}_i - \vec{R}_j}{|\vec{R}_i - \vec{R}_j|^3}, \quad i = 1,\ldots,N, \tag{77}$$

where the pseudo-oscillator frequencies ω_x, ω_y, and ω_z are defined in (19), and [12]

$$\xi_i(t) = -\frac{q}{2}X_i(t)\sin(2t), \quad \eta_i(t) = -\frac{q}{2}Y_i(t)\sin(2t),$$
$$\zeta_i(t) = qZ_i(t)\sin(2t). \tag{78}$$

Apparently, the main effect of the pseudopotential approximation is to *represent* (not eliminate) the effect of the rapid micromotion in the equations of the macromotion (77) by time-independent force terms, derived from an effective potential, the pseudopotential. In our experience this method is highly accurate as long as (i) q is small [see [18] and the fact that the ratios of the micromotion and macromotion amplitudes in (78) are proportional to q] and (ii) the trap frequency is large compared to the pseudo-oscillator frequencies ω_x, ω_y, and ω_z. In fact, in our experience, $q < 1/2$ and a ratio of 2:1 for the ratio of trap frequency and pseudo-oscillator frequencies are sufficient to guarantee acceptable accuracy. Since the set of equations (1) is unstable for $q \gtrsim 0.45$ (Mathieu stability limit), for stable three-dimensional trapping the condition $q < 1/2$ is automatically satisfied. Since for spherical clouds $\omega \approx q$, and since in our units the trap frequency is equal to 2, the other condition is also fulfilled. The accuracy of the pseudopotential approximation improves quickly with decreasing q and increasing trap frequency. We conclude that, for the parameter sets used in this paper, the pseudopotential approximation is reliable.

The first time the pseudopotential approximation is used in this paper is in the derivation of (13). It is important to emphasize that (13) is not obtained by *discarding* the micromotion; it is derived taking full account of the micromotion by writing $\vec{x}_i(t)$ in the form (74), with the components of $\vec{\chi}(t)$ given by (78), and then processing the explicitly time-dependent terms originating from the micromotion $\vec{\chi}(t)$ explicitly and analytically.

In (14) we replaced time averages by ensemble averages, and a few comments concerning this procedure are in order. To start the discussion, it is important to point out that in our numerical simulations we do not make this approximation. The numerical data points in Fig. 1, e.g., are computed via time averages, as required. The replacement of time averages by ensemble averages is necessary only for our analytical calculations. In Sec. II we argued that, because of the chaotic nature of the trapped particles' dynamics [10], the replacement is most likely justified. While it is known that chaos does not necessarily imply ergodicity [19], it likely does so in the case of *hard chaos* [20], in which there are no regular islands in phase space. In our case, in the presence of weak damping, regular islands correspond to attractors. To the best of our knowledge, based on extensive experience with trapped-particle simulations, there is only a single attractor in phase space, the one that corresponds to the crystal state. Apart from this attractor, we never encountered any others (except for crystals with different geometric orderings that are close in phase space). In addition, the phase-space volume of the basin of attraction [20] of the crystal attractor is vanishingly small compared with the total accessible phase space. A rough upper bound for the ratio of the phase-space volume of the crystal basin, $\mathcal{V}_c$, to the total phase-space volume, $\mathcal{V}$, may be estimated in the following way. Let us assume that the ratio of the available spatial dimensions of a cloud to the spatial dimensions of the basin is 2:1 (a gross underestimate), and that the same is assumed for the velocities. Then, in the case of $N = 20$ particles, an upper bound for the ratio of the phase-space volumes is $\mathcal{V}_c/\mathcal{V} < [(1/2)^6]^{20} \approx 10^{-36}$. This shows that, while in the cloud state, the presence of the crystal

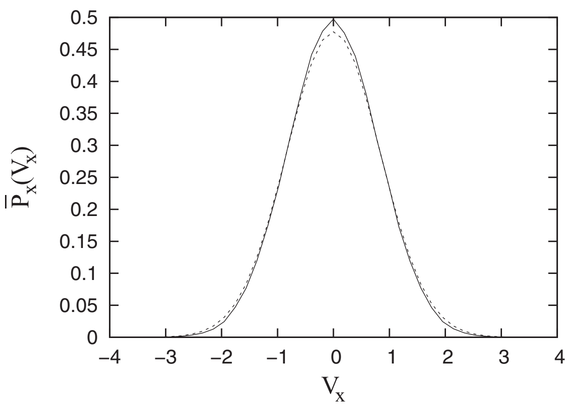

FIG. 4. Velocity distribution $\bar{P}_x(V_x)$ of $N = 20$ trapped particles (solid line) together with the theoretically expected Gaussian (dotted line), computed according to (25) with a temperature $\bar{T}$ extracted from the macromotion of the particles.

attractor is irrelevant for the cloud dynamics and therefore, for clouds, an assumption of ergodicity, allowing the approximate replacement of time averages with ensemble averages, is likely justified.

A final point concerns the notion of temperature in our manifestly time-dependent system. It is clear that a constant temperature cannot be defined for the trapped cloud during all phases of a trap cycle. According to (78), during a trap cycle, the cloud is first compressed in the radial direction while expanding in the z direction, and then it is compressed in the z direction while expanding in the radial direction. This is a nonequilibrium situation in which a temperature seemingly has no place. However, in the stationary state of a cloud, in which rf heating and cooling balance, the temperature of the macromotion is well defined [13]. It is the macromotion temperature, i.e., the thermal motion of $\vec{R}_i(t)$, that we refer to in our mean-field calculations. To test this picture, and to prove that the assumption of a Gaussian velocity distribution is valid, we computed, as an example, the distribution of the x component of the velocity of $N = 20$ trapped particles in the stationary state for the case $a = 0.02$, $q = 0.2$, and $\gamma = 4 \times 10^{-4}$. To improve the statistics we computed the combined ensemble and temporal average $\bar{P}_x(V_x)$ of the x component of the velocity distribution, defined as

$$\bar{P}_x(V_x) = \frac{1}{N}\sum_{i=1}^{N} \bar{p}_x(V_{i,x}), \tag{79}$$

where $p_x(V_{i,x})d^3\vec{V}$ is the probability of finding particle number i in the velocity volume element $d^3\vec{V}$, and the time average, in the stationary state, was extended over 10 000 trap cycles. Since our simulations return $\dot{x}_i(t)$, but not $\dot{X}_i(t)$, as required for the computation of $\bar{P}_x(V_x)$, we obtain $\dot{X}_i(t)$ by compensating for the micromotion. With (78) we have

$$V_{i,x} = \dot{X}_i(n\pi) = \dot{x}_i(n\pi) + q x_i(n\pi). \tag{80}$$

The solid line in Fig. 4 shows $\bar{P}_x(V_x)$, where the macromotion velocities $V_{i,x}$ were evaluated according to (80).

To compare with the theoretically expected Gaussian velocity distribution (25), we also computed the temperature

$$\bar{T} = \frac{1}{N}\sum_{i=1}^{N} \overline{\dot{X}_i^2} \tag{81}$$

as the temporal and ensemble average over all $N = 20$ particles and over 10 000 trap cycles, where the velocities $\dot{X}_i$ were again evaluated according to (80). Using $\bar{T}$ computed according to (81) in (25) with $l = x$, we obtain the Gaussian plotted as the dotted line in Fig. 4. We see that $\bar{P}_x$ and the Gaussian are reasonably close both in shape and in width. We note that there are no free parameters in this comparison, since the temperature, determining the width, is extracted from the numerical simulations as well. Thus the quantitative, parameter-free agreement between the two curves in Fig. 4 corroborates our assumption of (i) a Gaussian velocity distribution (agreement of shapes) and (ii) the notion of a temperature (agreement of widths).

VII. SUMMARY AND CONCLUSIONS

In this paper we provided the analytical underpinning of the scaling results found in [9]. We showed that a simple analytical mean-field theory is capable of explaining both existence and form of the universal heating curve [9]. The scaling we found is a consequence of the fact that both the pseudo-oscillator potential and the mean-field Coulomb potential are homogeneous functions of degrees 2 and -1, respectively. In addition we found an unexpected scaling that explains why the heating curve depends only on the single scaling parameter $\lambda = [q(N-1)]^{2/3}/T$. We observe excellent agreement between our analytical mean-field theory and the available numerical data.

ACKNOWLEDGMENT

R.B. acknowledges financial support by Grant No. 216687 of the Research Council of Norway.

[1] W. Paul, Rev. Mod. Phys. **62**, 531 (1990).

[2] C. W. Chou, D. B. Hume, J. C. J. Koelemeij, D. J. Wineland, and T. Rosenband, Phys. Rev. Lett. **104**, 070802 (2010).

[3] D. Leibfried, E. Knill, S. Seidelin, J. Britton, R. B. Blakestad, J. Chiaverini, D. B. Hume, W. M. Itano, J. D. Jost, C. Langer, R. Ozeri, R. Reichle, and D. J. Wineland, Nature (London) **438**, 639 (2005).

[4] H. G. Dehmelt, Adv. At. Mol. Phys. **3**, 53 (1967); **5**, 109 (1969).

[5] R. F. Wuerker, H. Shelton, and R. V. Langmuir, J. Appl. Phys. **30**, 342 (1959).

[6] R. Blatt, P. Gill, and R. C. Thompson, J. Mod. Opt. **39**, 193 (1992).

[7] H. J. Metcalf and P. van der Straten, *Laser Cooling and Trapping* (Springer, New York, 1999).

[8] D. A. Church, J. Mod. Opt. **39**, 423 (1992).
[9] J. D. Tarnas, Y. S. Nam, and R. Blümel, Phys. Rev. A **88**, 041401 (2013).
[10] R. Blümel, J. M. Chen, E. Peik, W. Quint, W. Schleich, Y. R. Shen, and H. Walther, Nature (London) **334**, 309 (1988).
[11] R. Blümel, C. Kappler, W. Quint, and H. Walther, Phys. Rev. A **40**, 808 (1989).
[12] L. D. Landau and E. M. Lifshits, *Mechanics*, 2nd ed. (Pergamon Press, Oxford, 1976).
[13] J. P. Schiffer, M. Drewsen, J. S. Hangst, and L. Hornekr, Proc. Natl. Acad. Sci. USA **97**, 10697 (2000).
[14] *Handbook of Mathematical Functions*, edited by M. Abramowitz and I. A. Stegun (National Bureau of Standards, Gaithersburg, MD, 1964).
[15] R. Bilato and M. Brambilla, Plasma Phys. Control. Fusion **46**, 1455 (2004).
[16] I. Siemers, R. Blatt, Th. Sauter, and W. Neuhauser, Phys. Rev. A **38**, 5121 (1988).
[17] R. G. Brewer, J. Hoffnagle, R. G. DeVoe, L. Reyna, and W. Henshaw, Nature (London) **344**, 305 (1990).
[18] F. G. Major, V. N. Gheorghe, and G. Werth, *Charged Particle Traps* (Springer, Berlin, 2005).
[19] J. L. Lebowitz and O. Penrose, Phys. Today **26**, 23 (1973).
[20] E. Ott, *Chaos in Dynamical Systems* (Cambridge University Press, Cambridge, UK, 1993).